

1    **Contrasting fast precipitation responses to tropospheric and stratospheric ozone forcing**

2    C. R. Macintosh, R. P. Allan, L. H. Baker, N. Bellouin, W. Collins, Z. Mousavi and K. P.

3    Shine

4    Department of Meteorology, University of Reading, Reading RG6 6BB, UK

5    Corresponding author: Keith P Shine, Department of Meteorology, University of Reading,

6    Reading RG6 6BB, UK. (k.p.shine@reading.ac.uk)

7    Submitted to *Geophysical Research Letters* 28 September 2015

8    Revised and resubmitted 3 December 2015

9    **Key Points**

- 10        • Fast precipitation response to ozone change simulated in a global climate model
- 11        • Fast precipitation responses to tropospheric and stratospheric O<sub>3</sub> change oppose each
- 12        other
- 13        • Simple model indicates present-day precipitation change due to O<sub>3</sub> could exceed 50%
- 14        of that from CO<sub>2</sub>

## Abstract

The precipitation response to radiative forcing (RF) can be decomposed into a fast precipitation response (FPR), which depends on the atmospheric component of RF, and a slow response, which depends on surface temperature change. We present the first detailed climate model study of the FPR due to tropospheric and stratospheric ozone changes. The FPR depends strongly on the altitude of ozone change. Increases below about 3 km cause a positive FPR; increases above cause a negative FPR. The FPR due to stratospheric ozone change is, per unit RF, about 3 times larger than that due to tropospheric ozone. As historical ozone trends in the troposphere and stratosphere are opposite in sign, so too are the FPRs. Simple climate model calculations of the time-dependent total (fast and slow) precipitation change, indicate that ozone's contribution to precipitation change in 2011, compared to 1765, could exceed 50% of that due to CO<sub>2</sub> change.

Index Terms: 1655 Water cycles; 3354 Precipitation; 3359 Radiative processes; 3362 Stratosphere-Troposphere Interactions

## 1. Introduction

Recent research [e.g. *Allen and Ingram, 2002; Ming et al. 2010; O’Gorman et al. 2012*] has created a framework, based on energetic constraints, for understanding the global precipitation response to climate perturbations. A simple model has been developed [e.g. *Allan et al. 2014; Ming et al. 2010; Thorpe and Andrews, 2014*] that relates the component of top-of-atmosphere radiative forcing ( $RF$ ) that directly affects the atmosphere ( $RF_{atm}$ ), surface temperature change ( $\Delta T$ ) and global-mean precipitation change ( $\Delta P$ ). This distinguishes between a *slow* precipitation response (SPR), related to  $\Delta T$ , and a *fast* precipitation response (FPR), involving rapid atmospheric adjustments over a period of days

and months, related to  $RF_{atm}$  and the fast response of surface sensible heat (SH) fluxes ( $\Delta SH_{fast}$ ), so that

$$L\Delta P = SPR + FPR \approx k\Delta T - (RF_{atm} + \Delta SH_{fast}). \quad (1)$$

$L$  is the latent heat of vaporization and  $k$  is a model-dependent constant. This relationship arises because, to first order, net radiative cooling is balanced by latent heating due to condensation [e.g. *Mitchell et al.*, 1987]. In steady state, the net rate of condensation equals the global-mean precipitation. In response to a forcing, the net atmospheric radiative cooling (and hence the precipitation) responds to both  $RF_{atm}$ , and the subsequent climate response.

We consider  $RF_{atm}$  in terms of  $RF$  using a parameter  $f$  (so that  $f = RF_{atm}/RF$ ) which is the fraction of  $RF$  felt directly by the atmosphere;  $k\Delta T$  represents the slow response arising from changes in atmospheric temperature, humidity and cloudiness due to  $\Delta T$ .  $k$  can be derived from climate model simulations, and may incorporate the slow SH response [*Lambert and Webb*, 2008; *Andrews et al.*, 2010].  $\Delta SH_{fast}$  is normally smaller than  $L\Delta P$ , and was not included in previous analyses [e.g. *Allan et al.*, 2014; *Thorpe and Andrews*, 2014], but will be computed here. We use two forms of  $RF$  [*Myhre et al.*, 2013]. The more traditional  $RF$  (with stratospheric temperature adjustment) is used for illustrative calculations in Section 2. Effective  $RF$  (ERF), which accounts for fast atmospheric adjustments to  $RF$ , is used in climate model simulations in Sections 3.

Climate model simulations [*Andrews et al.*, 2010; *Kvalevåg et al.*, 2013] show that  $f$  depends on the species under consideration. To our knowledge, *Andrews et al.* [2010] is the only study to quantify  $f$  for ozone. For total (pre-industrial to present-day) ozone changes they found that  $f$  was negative (-0.3) and so  $FPR$  and  $SPR$  are the same sign; by contrast they found  $f = 0.8$  for  $CO_2$ , so that  $FPR$  opposes  $SPR$ . Ozone's potential importance can be illustrated by computing the equilibrium  $\Delta P$  to present-day  $RF$ ; from Eq. (1) this is  $RF(k\lambda - f)$  (neglecting

$\Delta SH_{fast}$  for simplicity) [Shine *et al.* 2015], where  $\lambda$  is the climate sensitivity parameter. Using the Andrews *et al.* [2010]  $f$  factors, the 2011 RF values from Myhre *et al.* [2013] for total ozone and CO<sub>2</sub> (0.35 and 1.82 W m<sup>-2</sup> respectively), a mid-range  $\lambda$  of 0.8 K (W m<sup>-2</sup>)<sup>-1</sup> (assuming it is the same for ozone and CO<sub>2</sub>) and  $k = 2.2$  K (W m<sup>-2</sup>)<sup>-1</sup> (see section 4), ozone's equilibrium  $\Delta P$  is about 40% that of CO<sub>2</sub>; this is disproportionately strong compared to the RF (and equilibrium  $\Delta T$ ), where ozone's effect is 20% that of CO<sub>2</sub>.

This letter distinguishes, for the first time, between the FPR for stratospheric and tropospheric ozone perturbations and explains their combined response. This is important as the time variation of stratospheric and tropospheric ozone, and their RF, is quite different [e.g. Myhre *et al.*, 2013] because they respond to different drivers; hence a single value of  $f$  for ozone is unlikely to be applicable at all times. We first use radiation-only calculations to illustrate how  $RF_{am}$ , depends on the height of the ozone perturbation. These provide a platform for interpreting the response of an atmospheric general circulation model (GCM) which explicitly simulates the FPR. The first set of GCM calculations uses idealised ozone perturbations, particularly to explore the opposing FPR responses of lower and upper tropospheric ozone change and the amplified impact of stratospheric ozone changes, which are suggested by the radiation-only calculations. The second set uses more-realistic ozone perturbations, to quantify the FPR in response to historical ozone changes and to derive representative values for  $f$ . We then use these values in a simple global-mean model of historical precipitation change which includes both the FPR and SPR (Eq. 1) to contrast the roles of tropospheric and stratospheric ozone change, and compare them CO<sub>2</sub>.

This paper focuses largely on the relationship between global precipitation response and the global atmospheric energy balance. Ozone forcing can, via both the global response and changes in local circulation, induce changes in regional precipitation that are discussed

elsewhere [e.g. *Kang et al. 2011; Shindell et al., 2012; Marvel and Bonfils, 2013; Delworth and Zeng, 2014*].

## **2. Atmospheric radiative forcing as a function of the altitude of ozone perturbation**

Assuming the thermal infrared is the most height-dependent component of RF (as will be shown below), a simple conceptual model can be used to anticipate the response. The net effect of an increase in ozone depends on competition between increased atmospheric absorption of surface-emitted radiation (causing a positive  $RF_{\text{atm}}$ ) and increased atmospheric emission (causing a negative  $RF_{\text{atm}}$ ). In the warm lower troposphere, the emission term is likely the largest; in the colder upper troposphere, the absorption term is likely more important. Simple grey-body considerations (see Supporting Information) indicate that the  $RF_{\text{atm}}$  is likely to change sign in the mid-troposphere. Such a sign change (at around 700 hPa) has previously been shown, using detailed calculations, in response to increased water vapor amounts [*Previdi, 2010*].

A set of idealized radiation-only perturbation experiments are performed in which ozone is increased by 20% in each atmospheric layer in turn. RF,  $RF_{\text{atm}}$  and  $f$  are calculated for both cloud-free and all-sky cases using the *Edwards and Slingo [1996]* radiation code with 9 longwave and 6 shortwave spectral bands. The day-averaged shortwave calculations use mid-month conditions and a 6-point Gaussian integration over daylight hours. Calculations are performed on a  $2.5^\circ \times 3.75^\circ$  horizontal grid at 22 levels, using temperatures and humidity climatologies described in *MacIntosh et al. [2015]*. The zonal-mean ozone distribution is taken from the Atmospheric Chemistry and Climate Model Intercomparison Project (ACCMIP) multi-model-mean (not including the MOCAGE model in the stratosphere, where it is an outlier) [*Young et al., 2013*] and is based on year 2000 ozone precursor emissions and concentrations of ozone-depleting substances. Stratospheric temperature adjustment is

applied using fixed-dynamical heating with a  $2 \text{ K km}^{-1}$  tropopause definition. Annual-means are derived from averaging monthly-mean calculations for January, April, July and October. Some sensitivity to these specifications can be anticipated, but the prime purpose is to illustrate the driving physics, to help anticipate and interpret the GCM calculations in Section 3.

Figure 1a shows the strong dependence of  $\text{RF}_{\text{atm}}$  on the height of ozone perturbation, with only a small dependence on whether clouds are present. The variation with height in the troposphere is largely driven by the longwave (Fig. 1b). However, the shortwave perturbation strongly modifies where  $\text{RF}_{\text{atm}}$  changes sign and its magnitude, particularly in the upper troposphere and lower stratosphere.  $\text{RF}$  itself (Fig. 1c) also depends on the height of the ozone perturbation but it remains positive throughout the troposphere and lower stratosphere; it only becomes negative in the upper stratosphere [e.g. *Lacis et al.*, 1990] above the region of interest here. Hence,  $f$  depends strongly on the vertical distribution of ozone change (Fig. 1d) and changes sign at about 650 hPa. Because  $\Delta T$ , driven by  $\text{RF}$ , is positive for an ozone increase, the associated FPR will enhance the SPR for lower tropospheric ozone increases but oppose it for increases at higher altitudes.

For stratospheric ozone increases, the atmosphere as a whole gains energy due to increased SW absorption; this is opposed by increased LW emission, mostly as a result of the increase in stratospheric temperature in response to the SW absorption. Further analysis shows that the tropospheric energy gain, in this case, is primarily due to increased LW emission from the warmed stratosphere, as the SW absorbed by the troposphere decreases for this case. For tropospheric ozone increases, the increased SW absorption results in a tropospheric energy gain; whether the atmosphere as a whole gains or loses LW energy depends on the altitude of the ozone change.

### 3. Climate model simulations of the fast precipitation response to ozone change

We test the link between ERF and FPR using the atmosphere-only version of the HadGEM3 climate model, with a resolution of  $1.875^\circ \times 1.25^\circ$  and 63 vertical levels between the surface and 40 km [Hewitt *et al.*, 2011]. It also uses the *Edwards and Slingo* [1996] radiation scheme. Model winds above the boundary layer are relaxed towards ERA-Interim analyses following the method of *Telford et al.* [2008]. This experimental set-up allows relatively short model integrations which produce ERF's very similar to those from longer (20 year) integrations using an unconstrained model [Bellouin *et al.*, manuscript in preparation]. By not relaxing temperatures, the fast adjustments are less constrained, but there will be some suppression of the dynamical response. Simulations are run for 3 years (2008-2010) with sea surface temperatures (SSTs) and sea ice from the AMIP climatology [Reynolds *et al.*, 2007]. Fixing SSTs inhibits the SPR, although land temperatures remain free to adjust. ACCMIP ozone fields (Section 2) were imposed as monthly-varying zonal-mean climatologies. Forcings are presented as 3-year averages; the range that encompasses the forcings for individual years is shown, to indicate the robustness of the 3-year mean.

#### 3.1 Idealized ozone perturbations

A control simulation was conducted with the year 2000 ACCMIP ozone climatology (Section 2). Idealized simulations were then run by doubling ozone mixing ratios between the surface and 700 hPa (labeled Lower Troposphere, LT), between 700 hPa and the tropopause (Upper Troposphere, UT), and between the surface and the tropopause (LT+UT) to test the additivity of the UT and LT responses. For the stratosphere perturbation (ST) ozone mixing ratios were decreased by 20% between the tropopause and the model top. The 150 nmol mol<sup>-1</sup> ozone contour was used to identify the tropopause in the simulations.

Table 1 shows the global-mean results for these experiments for ERF,  $\text{ERF}_{\text{atm}}$ ,  $\Delta SH_{\text{fast}}$  and  $f$  (from  $\text{ERF}_{\text{atm}}/\text{ERF}$ ). The validity of the simple FPR model (Eq. 1) is assessed by comparing the predicted FPR due to  $\text{ERF}_{\text{atm}} + \Delta SH_{\text{fast}}$  with the GCM-simulated change in precipitation (converted to units of  $\text{W m}^{-2}$ ).

Table 1 shows that LT causes a positive FPR whereas UT causes a negative FPR despite ERF being positive for both cases. The ST experiment causes a positive FPR; because this is for an ozone decrease, the sense of the response (ozone increase leads to negative FPR) is the same as for UT.  $\text{ERF}_{\text{atm}} + \Delta SH_{\text{fast}}$  predict this behavior well, supporting the utility of Eq. (1);  $\Delta SH_{\text{fast}}$  is quite significant in size, typically 20-30% of  $\text{LAP}$ . The sign difference between the LT and UT FPR is as anticipated from Fig. 1, showing that the behavior is understood. LT+UT is within 5% of the sum of LT and UT, and shows that UT dominates.  $f$  varies strongly with height; it is largest for ST, and positive in all cases except LT. The FPR for ST is, per unit ERF, roughly 4 times larger than the FPR for LT+UT.

We briefly discuss the annual- and zonal-mean latitudinal distribution of FPR, and the role of cloud changes in influencing ERF. Figures 2a, 2d and 2g show the structure of  $\text{ERF}_{\text{atm}}$  (for clear-sky and all-sky cases) and the change in cloud radiative forcing between the control and perturbed cases. Clear and all-sky ozone forcings differ, because clouds strongly modulate the shortwave and longwave RF [e.g. *Berntsen et al.*, 1997]. Here the GCM results illustrate a marked difference between clear and all-sky ERFs (shown by the change in cloud forcing), particularly for LT (Fig. 2a), which is larger than anticipated from the RF calculations (Fig. 1). This indicates a significant fast cloud adjustment to the ozone perturbation, which modifies the  $\text{ERF}_{\text{atm}}$  and acts in addition to  $\text{RF}_{\text{atm}}$ .

Figures 2b, 2e and 2h show that precipitation changes occur largely in the tropics in all cases, and illustrate further the contrasting response of precipitation to LT and UT/ST ozone



changes. Figures 2c, 2f and 2i show indicators of cloud response in the model, the change in mid plus high and low cloud fraction (to distinguish between cloud within and above the boundary layer). The response is complex, and merits detailed study but, for all three simulations, a similar signature to the tropical precipitation change can clearly be seen in the mid plus high cloud fraction.

### 3.2 More-realistic ozone perturbations

We now consider more realistic ozone changes between the pre-industrial (1850) and the present-day (2000) atmosphere, derived from ACCMIP multi-model means (see Section 2). The control simulation uses 1850 ozone. Three perturbations are performed. “TROP” uses year 2000 tropospheric ozone; “STRAT” uses year 2000 ozone above the tropopause; “FULL” uses year 2000 ozone throughout the atmosphere. Since GCM runs are inherently noisy, we increased the TROP forcing to amplify the signal, by perturbing ozone by twice its historical change. The results presented here are divided by 2; we tested the linearity via off-line radiation calculations; for ozone perturbations of this size,  $RF_{atm}$  is linear to better than 1%.

Table 1 shows that TROP causes a negative FPR. Hence for more realistic ozone changes, as well as the idealized ones (Section 3.1), upper tropospheric changes are more influential than lower troposphere changes. STRAT causes a positive FPR and, as in the idealized experiments, with  $f$  much larger (by about a factor of 3 here) than for tropospheric ozone changes. The FULL FPR response is approximately the sum of the individual STRAT plus TROP experiments.  $ERF_{atm} + \Delta SH_{fast}$  is again a good indicator of FPR, with  $\Delta SH_{fast}$  accounting for 20-30% of  $L\Delta P$ . Figure S1 shows the equivalent plot to Fig. 2 for these simulations, and has broadly the same patterns; the signal is noisier because ozone and ERF changes are smaller (see Table 1).

The resulting FULL  $\text{ERF}_{\text{atm}}$  is positive, but small, and  $f$  is close to zero. The FPR due to stratospheric and tropospheric ozone changes strongly oppose each other in present-day conditions, despite the tropospheric ozone ERF being about 3.5 times the stratospheric ozone ERF.

These results contrast with Andrews et al. [2010] who find a net ozone RF of  $0.16 \text{ W m}^{-2}$  for the pre-industrial to 1990 period (compared to  $0.26 \text{ W m}^{-2}$  found here for FULL), and  $f$  of  $-0.3$ ; this suggests that, in their calculation, stratospheric ozone depletion is a larger component of RF.

We are unaware of any other ERF calculations for ozone, but our ERFs are broadly consistent with the RFs in Stevenson et al. [2013] and Conley et al. [2013] as used in Myhre et al. [2013]. For tropospheric ozone Stevenson et al. [2013] give an RF of  $0.34 \text{ W m}^{-2}$  for the same 1850-2000 dataset compared with our ERF of  $0.36 \text{ W m}^{-2}$ . For stratospheric ozone Conley et al. [2013] calculate an RF of  $-0.02 \text{ W m}^{-2}$  using a single radiation code applied to ozone changes from several ACCMIP models; Myhre et al. [2013] assess the 1750-2011 RF to be  $-0.05$  (range  $-0.15$  to  $+0.05 \text{ W m}^{-2}$ ) compared with the ERF of  $-0.1 \text{ W m}^{-2}$  derived here.

Repeating the equilibrium  $\Delta P$  calculation in Section 1, but using the  $f$  values derived here for stratospheric and tropospheric ozone (and the separate 2011 RFs of  $0.05$  and  $0.40 \text{ W m}^{-2}$  respectively [Myhre et al., 2013]) yields a reduced proportion to the  $\text{CO}_2$  change of 33% compared to 40% in Section 1, because the FPR no longer enhances the SPR. Nevertheless, this remains disproportionately strong compared to the RFs.

#### **4. Simple model calculations of total precipitation response**

To investigate the impact of these  $f$  values on the time-varying total precipitation response, we use the simple model approach of Allan et al. [2014] which incorporates the SPR and

FPR. As in *Thorpe and Andrews* [2014] and *Allan et al.* [2014],  $\Delta SH_{fast}$  is not included, given the illustrative nature of the calculations, but could reduce the ozone FPR by about 20%.

To compute the time-varying SPR, temperature is calculated with a simple global-mean model, with a mixed-layer ocean connected to a deep ocean via diffusion. These temperatures, and the  $f$  values from Section 3.2, are used to calculate the precipitation response using Eq. (1). A mid-range climate sensitivity of  $0.8 \text{ K (W m}^{-2}\text{)}^{-1}$  [*IPCC, 2013*] is used (and assumed to be the same for all forcing components).  $k$  is taken to be  $2.2 \text{ W m}^{-2} \text{ K}^{-1}$ , consistent with the multi-model mean value in *Previdi* [2010] and *Thorpe and Andrews* [2014], and includes the slow component of  $\Delta SH$ . The SPR, and hence the relative importance of the FPR, depends strongly on the choice of  $\lambda$  [e.g. *Shine et al.* 2015] and  $k$ .

The 1765-2011 tropospheric and stratospheric ozone RFs are taken from *IPCC* [2013 Appendix AII.1.2]. These are used to directly calculate the time-varying FPR; as explained in Section 3.2, these do not exactly correspond to the forcings derived from the more-realistic ozone GCMs perturbations, so the present-day FPRs differ slightly from Table 1 (and differ because  $\Delta SH_{fast}$  is neglected in the simple model). The precipitation response is compared with that for  $\text{CO}_2$  (assuming  $f=0.8$  [*Andrews et al.*, 2010] and the *IPCC* [2013]  $\text{CO}_2$  RFs), and for ozone but assuming the *Andrews et al.* [2010]  $f=-0.3$  for both tropospheric and stratospheric ozone.

Figure 3a shows the total ozone-related precipitation response and the FPR using  $f=-0.3$ . In this case, the tropospheric ozone FPR is positive, enhancing the SPR, while the stratospheric ozone FPR and total response is negative. Figure 3b is the same as Fig. 3a but uses the new  $f$  values for tropospheric and stratospheric ozone. In contrast to Fig. 3a, since the tropospheric ozone FPR now opposes the SPR, the total response is reduced, by a quarter in 2011. By contrast, the FPR is so strong for stratospheric ozone that it overwhelms the SPR, causing a

small precipitation increase. Figure 3c shows the SPR and FPR for CO<sub>2</sub> and tropospheric ozone using the  $f$  value derived here, to emphasize the strong compensation between the SPR and FPR components for CO<sub>2</sub>.

Although the total ozone  $\Delta P$  is now smaller than when using  $f=-0.3$ , Fig. 3b shows that it remains a large fraction of the CO<sub>2</sub>  $\Delta P$  (about 70% in 2011) despite the RF being only about 20% that of CO<sub>2</sub>. It is also significantly stronger than the value of 33% of equilibrium  $\Delta P$  derived in Section 3.2. This is because, in a transient calculation, the SPR, which drives the positive  $\Delta P$  for CO<sub>2</sub> and tropospheric ozone, is not fully expressed (unlike the FPR), as the temperature change is not in equilibrium with the RF. Since the FPR is proportionately more important in suppressing precipitation for CO<sub>2</sub> than tropospheric ozone, (Fig. 3c), the ozone total  $\Delta P$  is a larger fraction of that for CO<sub>2</sub> in the transient case. The relative importance of tropospheric ozone is also slightly larger because, in 2011, its  $\Delta T$  (and hence its SPR) is closer to equilibrium (about 67%) than CO<sub>2</sub> (about 60%) because the ozone forcing is, in relative terms, increasing less rapidly than the CO<sub>2</sub> forcing.

The results emphasize the need to treat tropospheric and stratospheric ozone separately in simple models. The time variation of stratospheric ozone can be seen to have some influence on recent precipitation changes, accelerating it (relative to the troposphere-only case) during the 1980s, and opposing it after 2000. Using the “compound” value of  $f$  for present-day ozone forcing (about 0.02 from Table 1) would misrepresent the time evolution of the FPR, as it would be close to zero throughout the time period in Fig. 3.

## 5. Discussion

This work has presented the first detailed climate model calculations of the FPR for tropospheric and stratospheric ozone changes and further demonstrate the primary role of the atmospheric energy constraint in driving the FPR. As is clear from Table 1, across all the

277 GCM experiments discussed here,  $\Delta SH_{fast}$  offsets about 20% of the FPR that would result  
278 directly from  $RF_{atm}$ . This almost constant proportion contrasts with the absorbing aerosol case  
279 of *Ming et al.* [2010] where  $\Delta SH$  (and, they argue,  $\Delta SH_{fast}$ ) became the dominant term in  
280 balancing  $RF_{atm}$  when aerosol was located in the boundary layer. The contrasting behaviour  
281 may be because our ozone perturbations are rather deep (extending to 700 hPa in the LT case)  
282 or it may be related to the differences in the impact of ozone and aerosol on  $RF_{atm}$ .

283 This study demonstrates that the FPR for changes in lower tropospheric ozone is the same  
284 sign as the SPR, while for upper tropospheric and stratospheric ozone changes, it is of  
285 opposite sign. Radiation-only calculations demonstrate the reasons originate in the balance  
286 between the change in absorption and emission of infrared radiation modified by the change  
287 in absorption of solar radiation. For more realistic ozone changes, the FPR for tropospheric  
288 ozone overall acts to oppose the SPR, as it does for stratospheric ozone; however, since the  
289 historical changes in tropospheric and stratospheric ozone (and their RFs) are of opposite  
290 signs, so too are their FPRs. Per unit radiative forcing, the FPR for stratospheric ozone  
291 changes are found to be 3 to 4 times larger than the tropospheric ozone FPR.

292 A simple model of the time-varying global-mean precipitation change, including the FPR and  
293 SPR, indicates that, for the model parameters chosen here, the present-day precipitation  
294 response to ozone change may exceed 50% of that due to  $CO_2$ , even though the RF is only  
295 about 20%. This is mostly because the compensation between the FPR and SPR is much  
296 stronger for  $CO_2$  than tropospheric ozone, and partly because stratospheric ozone depletion,  
297 despite its negative RF, causes precipitation increases. The results also indicate that, in simple  
298 model approaches, it is important to treat tropospheric and stratospheric ozone separately; the  
299 total ozone FPR depends on the balance of the strength of the individual tropospheric and  
300 stratospheric RFs which is very time dependent.

Clearly the analysis presented here is for a single GCM and for particular ozone perturbations; the response of other climate models would be of great interest. It also focuses on the global, rather than regional, responses. Nevertheless, the results highlight the opposing roles of stratospheric and tropospheric ozone in the FPR, the efficacy of stratospheric ozone in causing an FPR and show the overall impact of ozone change on global precipitation response may be substantial.

## References

- Allan, R. P., Liu, C. L., Zahn, M., Lavers, D. A., Koukouvagias, E., and Bodas-Salcedo, A.: Physically Consistent Responses of the Global Atmospheric Hydrological Cycle in Models and Observations, *Surveys in Geophysics*, 35, 533-552, 10.1007/s10712-012-9213-z, 2014.
- Allen, M. R., and Ingram, W. J.: Constraints on future changes in climate and the hydrologic cycle, *Nature*, 419, 224-232, 10.1038/nature01092, 2002.
- Andrews, T., Forster, P. M., Boucher, O., Bellouin, N., and Jones, A.: Precipitation, radiative forcing and global temperature change, *Geophysical Research Letters*, 37, 10.1029/2010gl043991, 2010.
- Berntsen, T., Isaksen, I., Myhre, G., Fuglestad, J., Stordal, F., Larsen, T., Freckleton, R., and Shine, K.: Effects of anthropogenic emissions on tropospheric ozone and its radiative forcing, *Journal of Geophysical Research-Atmospheres*, 102, 28101-28126, 10.1029/97JD02226, 1997.
- Conley, A. J., Lamarque, J. F., Vitt, F., Collins, W. D., and Kiehl, J.: PORT, a CESM tool for the diagnosis of radiative forcing, *Geoscientific Model Development*, 6, 469-476, 10.5194/gmd-6-469-2013, 2013.
- Delworth, T. L., and Zeng, F. R.: Regional rainfall decline in Australia attributed to anthropogenic greenhouse gases and ozone levels Latitude, *Nature Geoscience*, 7, 583-

326 587, 10.1038/ngeo2201, 2014.

327 Edwards, J. M., and Slingo, A.: Studies with a flexible new radiation code .1. Choosing a  
 328 configuration for a large-scale model, Quarterly Journal of the Royal Meteorological  
 329 Society, 122, 689-719, 10.1002/qj.49712253107, 1996.

330 Hewitt, H. T., Copsey, D., Culverwell, I. D., Harris, C. M., Hill, R. S. R., Keen, A. B.,  
 331 McLaren, A. J., and Hunke, E. C.: Design and implementation of the infrastructure of  
 332 HadGEM3: the next-generation Met Office climate modelling system, Geoscientific  
 333 Model Development, 4, 223-253, 10.5194/gmd-4-223-2011, 2011.

334 IPCC: Climate Change 2013: The Physical Science Basis. Contribution of Working Group I  
 335 to the Fifth Assessment Report of the Intergovernmental Panel on Climate Change,  
 336 Cambridge University Press, Cambridge, United Kingdom and New York, NY, USA,  
 337 1535 pp., 2013.

338 Kang, S. M., Polvani, L. M., Fyfe, J. C., and Sigmond, M.: Impact of Polar Ozone Depletion  
 339 on Subtropical Precipitation, Science, 332, 951-954, 10.1126/science.1202131, 2011.

340 Kvalevåg, M. M., Samset, B. H., and Myhre, G.: Hydrological sensitivity to greenhouse  
 341 gases and aerosols in a global climate model, Geophysical Research Letters, 40,  
 342 10.1002/grl.50318, 2013.

343 Lacis, A. A., Wuebbles, D. J., and Logan, J. A.: Radiative forcing of climate by changes in  
 344 the vertical-distribution of ozone, Journal of Geophysical Research-Atmospheres, 95,  
 345 9971-9981, 10.1029/JD095iD07p09971, 1990.

346 Lambert, F. H., and Webb, M. J.: Dependency of global mean precipitation on surface  
 347 temperature, Geophysical Research Letters, 35, 10.1029/2008gl034838, 2008.

348 MacIntosh, C. R., Shine, K. P., and Collins, W. J.: Radiative forcing and climate metrics for  
 349 ozone precursor emissions: the impact of multi-model averaging, Atmospheric Chemistry  
 350 and Physics, 15, 3957-3969, 10.5194/acp-15-3957-2015, 2015.

351 Marvel, K., and Bonfils, C.: Identifying external influences on global precipitation,  
 352 Proceedings of the National Academy of Sciences of the United States of America, 110,  
 353 19301-19306, 10.1073/pnas.1314382110, 2013.

354 Ming, Y., Ramaswamy, V., and Persad, G.: Two opposing effects of absorbing aerosols on  
 355 global-mean precipitation, *Geophys. Res. Lett.*, 37, L13701, doi:10.1029/2010gl042895,  
 356 2010.

357 Mitchell, J. F. B., Wilson, C. A., and Cunningham, W. M.: On CO<sub>2</sub> climate sensitivity and  
 358 model dependence of results, *Quarterly Journal of the Royal Meteorological Society*, 113,  
 359 293-322, 10.1256/smsqj.47516, 1987.

360 Myhre, G., Shindell, D., Bréon, F.-M., Collins, W., Fuglestad, J., Huang, J., Koch, D.,  
 361 Lamarque, J.-F., Lee, D., Mendoza, B., Nakajima, T., Robock, A., Stephens, G.,  
 362 Takemura, T., and Zhang, H.: Anthropogenic and Natural Radiative Forcing, in: *Climate*  
 363 *Change 2013: The Physical Science Basis. Contribution of Working Group I to the Fifth*  
 364 *Assessment Report of the Intergovernmental Panel on Climate Change*, edited by: Stocker,  
 365 T. F., Qin, D., Plattner, G. K., Tignor, M., Allen, S. K., Boschung, J., Nauels, A., Xia, Y.,  
 366 Bex, V., and Midgley, P. M., Cambridge University Press, Cambridge, United Kingdom  
 367 and New York, NY, USA, 659–740, 2013.

368 O'Gorman, P. A., Allan, R. P., Byrne, M. P. & Previdi, M.: Energetic constraints on  
 369 precipitation under climate change. *Surveys in Geophysics* 33, 585-608, 10.1007/s10712-  
 370 011-9159-6, 2012.

371 Previdi, M.: Radiative feedbacks on global precipitation, *Environmental Research Letters*, 5,  
 372 10.1088/1748-9326/5/2/025211, 2010.

373 Reynolds, R. W., Smith, T. M., Liu, C., Chelton, D. B., Casey, K. S., and Schlax, M. G.:  
 374 Daily high-resolution-blended analyses for sea surface temperature, *Journal of Climate*,  
 375 20, 5473-5496, 10.1175/2007jcli1824.1, 2007.



376 Rossow, W. B., and Schiffer, R. A.: Advances in understanding clouds from ISCCP, Bulletin  
 377 of the American Meteorological Society, 80, 2261-2287, 10.1175/1520-  
 378 0477(1999)080<2261:aiucfi>2.0.co;2, 1999.

379 Shindell, D. T., Voulgarakis, A., Faluvegi, G., and Milly, G.: Precipitation response to  
 380 regional radiative forcing, Atmospheric Chemistry and Physics, 12, 6969-6982,  
 381 10.5194/acp-12-6969-2012, 2012.

382 Shine, K.P., Allan R.P., Collins W.J., and Fuglestad, J.S.: Metrics for linking emissions of  
 383 gases and aerosols to global precipitation changes. Earth Syst. Dynam., 6, 525-540  
 384 doi:10.5194/esd-6-525-2015, 2015.

385 Stevenson, D. S., Young, P. J., Naik, V., Lamarque, J. F., Shindell, D. T., Voulgarakis, A.,  
 386 Skeie, R. B., Dalsoren, S. B., Myhre, G., Berntsen, T. K., Folberth, G. A., Rumbold, S. T.,  
 387 Collins, W. J., MacKenzie, I. A., Doherty, R. M., Zeng, G., van Noije, T. P. C., Strunk, A.,  
 388 Bergmann, D., Cameron-Smith, P., Plummer, D. A., Strode, S. A., Horowitz, L., Lee, Y.  
 389 H., Szopa, S., Sudo, K., Nagashima, T., Josse, B., Cionni, I., Righi, M., Eyring, V.,  
 390 Conley, A., Bowman, K. W., Wild, O., and Archibald, A.: Tropospheric ozone changes,  
 391 radiative forcing and attribution to emissions in the Atmospheric Chemistry and Climate  
 392 Model Intercomparison Project (ACCMIP), Atmospheric Chemistry and Physics, 13,  
 393 3063-3085, 10.5194/acp-13-3063-2013, 2013.

394 Telford, P. J., Braesicke, P., Morgenstern, O., and Pyle, J. A.: Technical Note: Description  
 395 and assessment of a nudged version of the new dynamics Unified Model, Atmospheric  
 396 Chemistry and Physics, 8, 1701-1712, 2008.

397 Thorpe, L., and Andrews, T.: The physical drivers of historical and 21st century global  
 398 precipitation changes, Environmental Research Letters, 9, 10.1088/1748-9326/9/6/064024,  
 399 2014.

400 Young, P. J., Archibald, A. T., Bowman, K. W., Lamarque, J. F., Naik, V., Stevenson, D. S.,

Tilmes, S., Voulgarakis, A., Wild, O., Bergmann, D., Cameron-Smith, P., Cionni, I.,  
Collins, W. J., Dalsoren, S. B., Doherty, R. M., Eyring, V., Faluvegi, G., Horowitz, L. W.,  
Josse, B., Lee, Y. H., MacKenzie, I. A., Nagashima, T., Plummer, D. A., Righi, M.,  
Rumbold, S. T., Skeie, R. B., Shindell, D. T., Strode, S. A., Sudo, K., Szopa, S., and Zeng,  
G.: Pre-industrial to end 21st century projections of tropospheric ozone from the  
Atmospheric Chemistry and Climate Model Intercomparison Project (ACCMIP),  
Atmospheric Chemistry and Physics, 13, 2063-2090, 10.5194/acp-13-2063-2013, 2013.

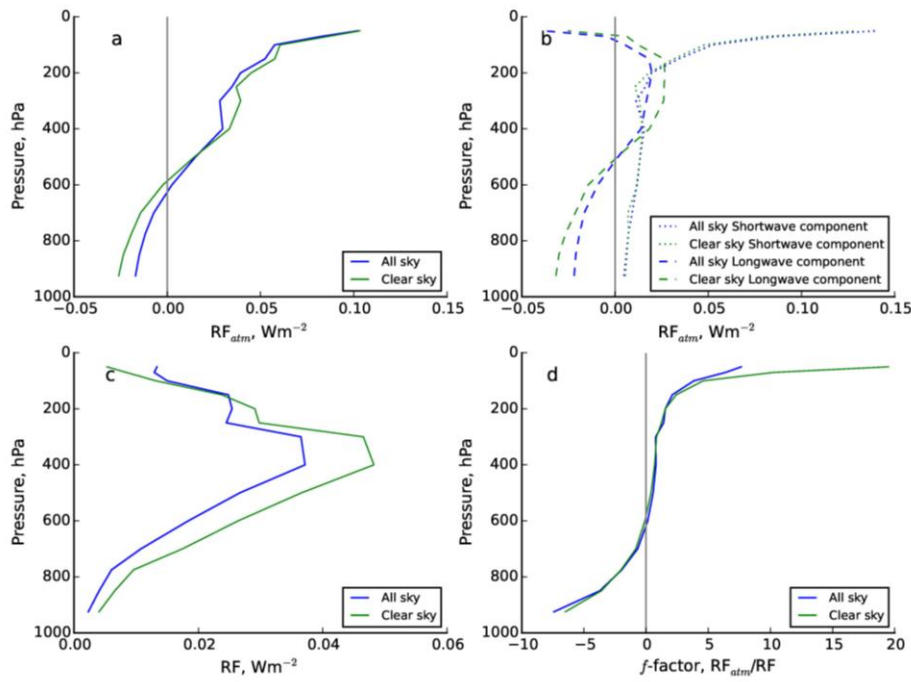
#### **Acknowledgements**

CM, LB, NB, WC and KS were supported by the European Commission's ECLIPSE  
(Evaluating the Climate and Air Quality Impacts of Short-Lived Pollutants) Project (Grant  
Agreement 282688). RA was supported by the UK Natural Environment Research Council  
DEEP-C project (NE/K005480/1) and the National Centre for Atmospheric Sciences. Tim  
Andrews and an anonymous reviewer are thanked for many helpful comments.

Table 1: Top-of-atmosphere and atmospheric effective radiative forcing, the fast sensible heat flux change, fast precipitation response (multiplied by the latent heat of vaporization) (all in  $\text{W m}^{-2}$ ) and  $f$  (i.e.  $\text{ERF}_{\text{atm}}/\text{ERF}$ ) for climate model simulations for 4 idealised (top rows) and 3 more realistic (bottom rows) ozone perturbations<sup>a</sup>. The fast precipitation response in  $\text{mm day}^{-1}$  is shown in parentheses.

Experiment	ERF ( $\text{W m}^{-2}$ )	$\text{ERF}_{\text{atm}}$ ( $\text{W m}^{-2}$ )	$\Delta\text{SH}_{\text{fast}}$ ( $\text{W m}^{-2}$ )	$\text{ERF}_{\text{atm}} + \Delta\text{SH}_{\text{fast}}$ ( $\text{W m}^{-2}$ )	FPR ( $\text{W m}^{-2}$ ) (and $\text{mm day}^{-1}$ )	$f$
Idealized						
UT+LT	$1.11 \pm 0.01$	$0.48 \pm 0.01$	$-0.11 \pm 0.01$	$0.37 \pm 0.01$	$-0.37 \pm 0.01$ (-0.013)	$0.43 \pm 0.01$
LT	$0.28 \pm 0.01$	$-0.12 \pm 0.01$	$0.02 \pm 0.01$	$-0.10 \pm 0.00$	$0.10 \pm 0.00$ (0.0034)	$-0.42 \pm 0.03$
UT	$0.83 \pm 0.01$	$0.58 \pm 0.01$	$-0.13 \pm 0.01$	$0.46 \pm 0.01$	$-0.45 \pm 0.00$ (-0.015)	$0.70 \pm 0.01$
ST	$-0.27 \pm 0.02$	$-0.46 \pm 0.02$	$0.10 \pm 0.00$	$-0.36 \pm 0.01$	$0.36 \pm 0.02$ (0.012)	$1.70 \pm 0.10$
More realistic						
FULL	$0.26 \pm 0.02$	$0.006 \pm 0.002$	$-0.009 \pm 0.005$	$-0.003 \pm 0.007$	$0.005 \pm 0.011$ (0.0017)	$0.02 \pm 0.01$
TROP	$0.36 \pm 0.00$	$0.13 \pm 0.01$	$-0.03 \pm 0.00$	$0.10 \pm 0.00$	$-0.10 \pm 0.01$ (-0.0034)	$0.36 \pm 0.01$
STRAT	$-0.096 \pm 0.026$	$-0.12 \pm 0.01$	$0.02 \pm 0.01$	$-0.10 \pm 0.01$	$0.10 \pm 0.01$ (0.0034)	$1.27 \pm 0.36$

<sup>a</sup>The results are the average of three years; the  $\pm$  range encompasses the values for each individual year.



429

430 Figure 1: Impact of 20% global increases in ozone applied in each atmospheric layer in turn  
 431 on RF,  $\text{RF}_{\text{atm}}$  and  $f$ . The vertical coordinate is the pressure at which the perturbation is  
 432 applied. a)  $\text{RF}_{\text{atm}}$ ; b) longwave (including stratospheric adjustment) and shortwave  
 433 components of a); c) RF; d)  $f = \text{RF}_{\text{atm}}/\text{RF}$ . Results are shown for clear and all-sky cases.

434

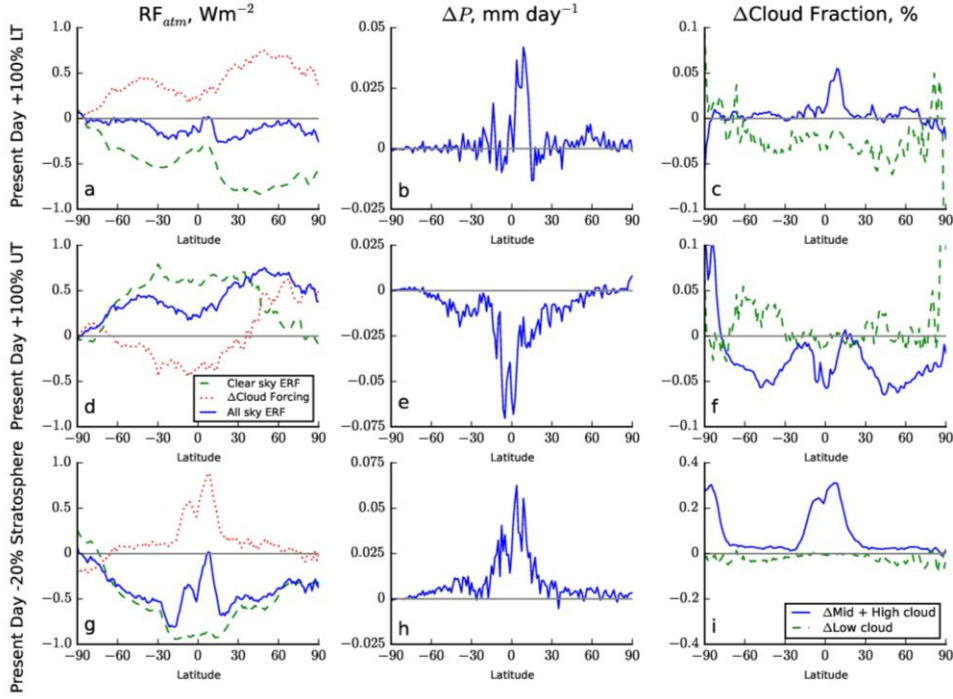


Figure 2: Zonal and annual-mean ERFs (left), precipitation changes (middle) and cloud changes (right) for the idealized ozone perturbation GCM simulations. Cloud responses are separated between below 2 km (“low”) and above 2 km (“Mid + High”). The LT, UT and ST simulations are in the top, middle and bottom rows respectively.

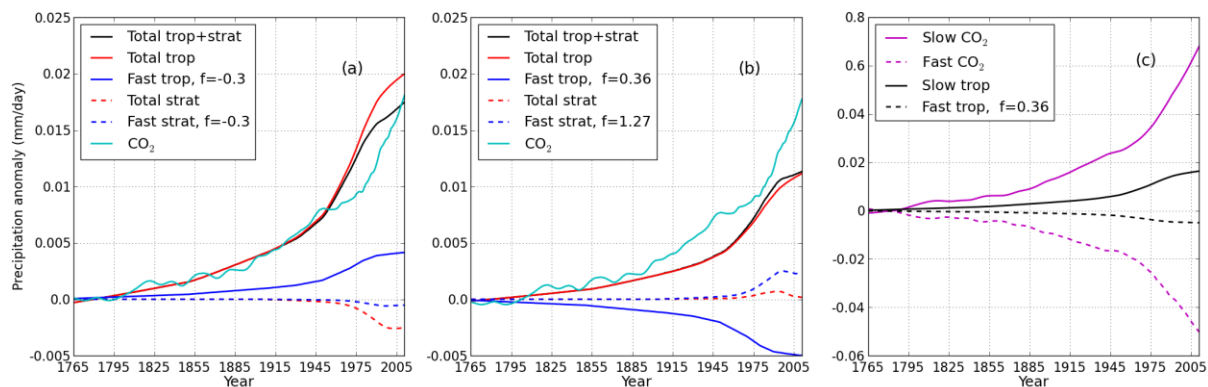


Figure 3: Simple model estimates of the global-mean precipitation response to ozone forcing using the IPCC AR5 radiative forcings from 1765 to 2010. a: Total and fast precipitation response to tropospheric, stratospheric ozone and both using  $f=-0.3$ . The total response to  $CO_2$  is also shown. b: As a, but using  $f=0.36$  for tropospheric and  $f=1.27$  for stratospheric ozone. c: The fast and slow components of the response for  $CO_2$  and tropospheric ozone.

**Contrasting fast precipitation response to tropospheric and stratospheric ozone forcing**

C. R. Macintosh, R. P. Allan, L. H. Baker, N. Bellouin, W. Collins, Z. Mousavi and K. P. Shine

Department of Meteorology, University of Reading, Reading RG6 6BB, UK

**Contents of this file**

Simple model derivation (including Figure S1) and Figure S2

**Introduction**

The supporting information contains a brief derivation, using a simple grey-body model, to illustrate the dependence of the longwave component of the atmospheric radiative forcing to the surface-atmosphere temperature difference and one further figure.

**Simple grey-body model of longwave component of the atmospheric radiative forcing**

In support of the discussion in Section 2, consider a single-layer atmosphere, with temperature  $T_a$  and emittance  $\epsilon$ , overlying a black-body surface of temperature  $T_s$  (see Figure S1).

The longwave radiation budget of this single-layer atmosphere is the net effect of absorption of infrared radiation emitted by the surface ( $\epsilon\sigma T_s^4$  since absorptance=emittance) and emission by the layer ( $2\epsilon\sigma T_a^4$ ).

If the emittance of this layer is changed by  $\Delta\epsilon$ , by, for example, changing the ozone concentration, then atmospheric radiative forcing  $RF_{atm}$  will be  $\Delta\epsilon\sigma(T_s^4 - 2T_a^4)$ . In this case if  $\Delta\epsilon$  is positive,  $RF_{atm}$  will be negative if  $T_a > 0.84T_s$ , as the increased atmospheric emission as a result of  $\Delta\epsilon$  exceeds the increased absorption of surface-emitted radiation, and vice versa if  $T_a < 0.84T_s$ .

From this we anticipate that the longwave component of  $RF_{atm}$  will be negative for ozone increases close to the surface, and positive for ozone increases away from the surface, as is indeed found in the detailed radiative calculations shown in Figure 1(a) of the paper.

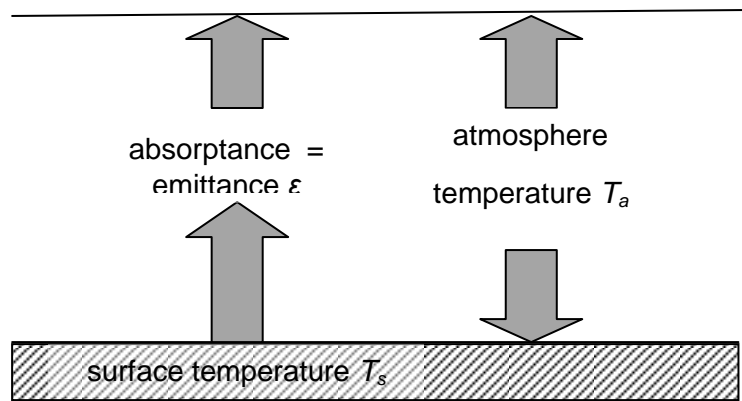


**Figure S1.** Schematic of simple grey-body single-layer atmosphere model to show the absorption of surface emitted radiation and the emission of radiation by the atmosphere.



## Figure S2

Figure S2 shows the zonal-mean and annual mean atmospheric component of the radiative forcing, precipitation changes and changes in low and mid-plus-high cloud for the more-realistic ozone perturbations described in Section 3.2 of the paper, and is the equivalent of Figure 2 in the paper that pertains to the idealized ozone perturbations. The FULL simulation perturbs ozone in the troposphere and stratosphere, STRAT perturbs it in the stratosphere only and TROP perturbs it in the troposphere only.

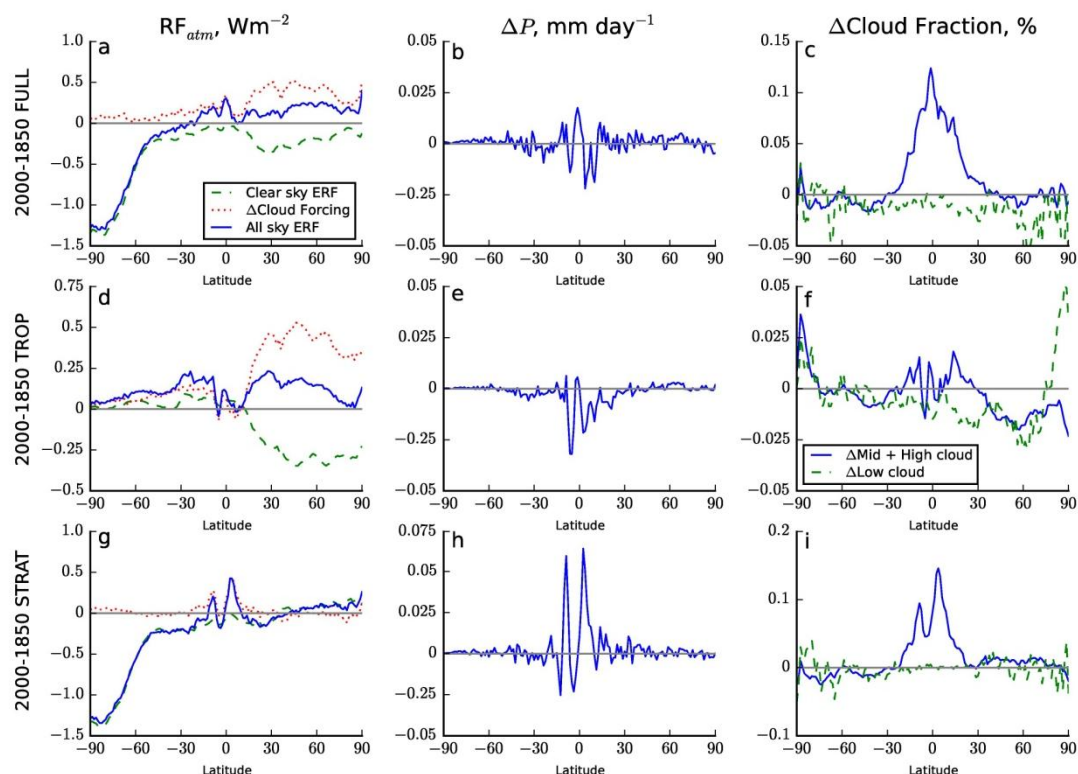


**Figure S2.** As Fig. 2, but for the more-realistic ozone perturbations. Zonal and annual-mean ERFs (left column), precipitation changes (middle column) and cloud changes (right column). Cloud responses are separated between those below 2 km (“low”) and above 2 km (“Mid + High”). The FULL simulations (see main text for explanation) are shown in the top row, the TROP (middle row) and STRAT (bottom row).